Computational Materials Science 172 (2020) 109290

Contents lists available at ScienceDirect

Computational Materials Science

journal homepage: www.elsevier.com/locate/commatsci

Multiscale modeling of copper and copper/nickel nanofoams under compression

H. Ke*, A. Garcia Jimenez, D.A. Rodrigues Da Silva, I. Mastorakos

Department of Mechanical and Aeronautical Engineering, Clarkson University, Potsdam, NY 13699, USA

ARTICLE INFO

Keywords:
Metallic nanofoam
Core/shell structure
Molecular dynamics
Finite element method

ABSTRACT

Pure metal nanofoams in the form of interconnected ligament networks have shown strong potential over the last few years in areas such as catalysts, batteries, and optics. However, they are often fragile and therefore difficult to integrate into engineering applications. For these reasons, a new class of materials, composite metallic nanofoams made of ligaments coated with thin metallic layers, have been proposed to solve these issue. The mechanical properties of these nanofoams depend on their relative density and their internal geometrical structure. In this work, we combine molecular dynamics (MD) and finite element method (FEM) to investigate the compressive behavior of nanofoams made of copper ligaments coated with nickel. We also investigate how this behavior relates to their microstructures. For that purpose, we built different types of representative cell structures, and atomistic simulations of multiaxial compression tests were performed to produce yield surfaces. Then the generated yield surfaces were curve fitted into a normalized model to obtain the shape parameters. Last, a plasticity model was introduced to study and compare their mechanical behavior under compression. The results suggest that the coating of the ligaments can improve the mechanical behavior of the nanofoams. They also reveal the importance and the limitations of the microstructural geometry on the strengthening of these structures. These findings can be used for the design of metallic nanofoams with tailored mechanical properties.

1. Introduction

Metallic nanofoams are made of materials such as copper (Cu), nickel (Ni), gold (Au) and platinum (Pt) in the form of interconnected networks of ligaments. They possess both the properties of metals, such as good electrical conductivity and ductility, and the properties of nano-architectures, such as high surface area, high surface to volume ratio and low relative density. These important properties make them a excellent alternative for a wide range of applications, such as catalysts [1,2], hydrogen storage foams [3,4], fuel cells [5,6], plasmonics [7] and dye-sensitized solar cells [8].

However, metallic nanofoams exhibit brittle behavior macroscopically due to plastic deformation in individual ligaments [9]. This lack of macroscopic strength is one of the limiting factors preventing their broad application. During the last few years, a considerable amount of effort has been devoted to study the mechanical properties of metallic nanofoams. Most of this work is either experimental [10] or computational [11,12] focusing on the nanoscale mechanisms without association to the macroscale. At the continuum level, the Gibson and Ashby model [13] was first used to estimate the yield strength and ultimate tensile strength by using the relationship between the relative density and the bulk material mechanical properties. However, this model is tuned to microscopic foams, and it does not apply to nanofoams, as it fails to consider the nanostructural parameters of ligaments constituting the nanofoam basis. As Hodge et al. reported [14], the yield strength of metallic nanofoams varies with the ligament diameter, and a modified scaling equation was proposed, which incorporates the ligament low densities and size effects. Moreover, Fan et al. [15] extended the model of Hodge for gold nanofoams at higher relative density, and Xia et al. [16] studied the surface effects on the effective mechanical behavior of nanoporous materials by a size-dependent Timoshenko nanobeam model. Finally, Feng et al. [17] examined the surface effect on the effective Young's modulus of open-cell nanoporous materials by adding a surface layer into the unit-cell micromechanics model.

Overall, the mechanical behavior of metallic nanofoams is determined by the relationship between the behavior of the individual ligaments of which this material is formed and their geometry. For this reason, in order to fabricate stronger nanofoams, the strength of their ligaments must be increased. However, although in pure metallic

* Corresponding author.
E-mail addresses: keh@clarkson.edu (H. Ke), garciaji@clarkson.edu (A.G. Jimenez), silvad@clarkson.edu (D.A.R. Da Silva), imastora@clarkson.edu (I. Mastorakos).

https://doi.org/10.1016/j.commatsci.2019.109290
Received 13 June 2019; Received in revised form 16 September 2019; Accepted 17 September 2019

nanofoams the ligament strength approaches the theoretical strength, their most significant impediment is their lack of ability to strain harden. This behavior is due to dealloying, the traditional manufacturing process of nanofoams, that makes strengthening mechanisms such as precipitation hardening, solid solution, and grain size strengthening impossible. An alternative technique has also been proposed that builds metal nanofoams using electrospinning [10]. It can form random nanofoams with porosities as high as 93%. However, the produced foams are still weak, although more ductile. Therefore, it is crucial to find an alternative solution to strengthen random nanofoams.

One method proposed to achieve the goal is by coating the individual ligaments with another metal, thus developing composite nanofoams [18]. The idea originated from the nanoscale metallic multilayers (NMM) materials, which have already shown significant improvement of high flow strength, good ductility and plastic flow stability due to the existence of interfaces within the structures [19–25]. The interfaces play various roles in determining the mechanical behavior of NMMs. Misra et al. [19] suggested that the mechanism responsible for their strengthening is the presence of coherency stresses produced by the small lattice mismatch between the two metals of the interface. The interfaces are barriers for impeding the propagation of dislocations inside the nanostructure because, in order to achieve slip transmission, they must overcome the coherency stresses. Abdolrahim et al. [12] reported that the strengthening effect of the Au-Ni nanofoams increases with the activity of the twins in Au-Ni ligaments, which gives rise to increased ductile behavior. Furthermore, Mastorakos et al. [26] concluded that composite Cu/Ni nanowires exhibit pseudoelastic behavior during loading due to the formation and subsequent propagation of twins, which could generate more plastic deformation and improve the ductility of the structures.

Most reported computational work on foams is focused either on the mechanical behavior of the nano-ligaments or on simplified geometrical models which neglect the atomistic configurations [13]. In this paper, we incorporate both these techniques to present a multiscale model for copper nanofoams that cover two length scales: atomistic and macroscopic. The purpose of the current study is to investigate how the relative density and internal geometrical structure influence the macroscopic mechanical behavior of copper nanofoam under compression. For this purpose, molecular dynamics simulations were performed in four different types of representative cell structures to obtain yield points for various load combinations under compression. The yield points were then curve fitted to the Deshpande theoretical model [27] to obtain yield surfaces. Finally, these yield surfaces were used in a plasticity model to simulate the macroscopic compressive behavior of metallic nanofoams. Although this work is mainly focused on high porosity metal nanofoams, like the ones produced by the electrospinning technique discussed above, it can also be applied to more traditional foams manufactured by the dealloying method.

2. Methodology

2.1. Nanofoam cell structures generation

First, several types of cell structures have been created to mimic the porous characteristic of metallic nanofoams. Previous studies have used various techniques to generate the metallic nanofoam structure. For example, Gunkelmann et al. [28,29] and Ke et al. [30] created the nanofoam from a perfect fcc crystal with periodic boundary conditions that it was then heated above the melting temperature. The nanofoams have been obtained by removing the atoms with temperatures above a determined value explicitly chosen to get the desired porosity. Crowson et al. [31,32] introduced a phase-field model to create gold nanofoams through the spinodal decomposition of a binary alloy. Their nanofoam samples have shown similar atomistic configurations with real experimental findings in terms of ligament size distribution and surface curvature. An alternative method uses atomistic Monte Carlo (MC) simulations of binary mixtures to generate nanofoams by spinodal decomposition [33,11]. All the above techniques produced random nanofoam structures with relative densities in the range of 40%–60%. The ratio of the number of atoms of the foam over the number of particles of the bulk material occupying the same volume defines the relative density. Due to their randomness, these structures cannot provide information about the effect of nanoligament connectivity and nanofoam local geometry on the strengthening of the nanofoams. As the nanofoams are made of nanoligaments connected randomly with each other forming numerous types of joints. The contribution of each joint to the macroscopic strength of the structure cannot be identified.

To resolve this issue, in this work, we propose a different approach. Instead of creating random structures, we generated geometric structures representing ordered periodic foam cells like these suggested in [13], with small modifications and differentiations to obtain the desired total number of ligaments linked to joints. Based on the specific geometric characteristics, each foam cell possesses certain mechanical

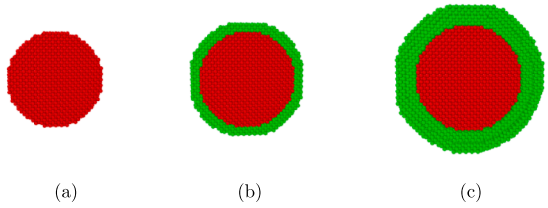

Fig. 1. The cross-section views of (a) pure copper ligaments and (b, c) composite Cu/Ni ligaments. The red and green atoms are corresponding to copper and nickel atoms, respectively.

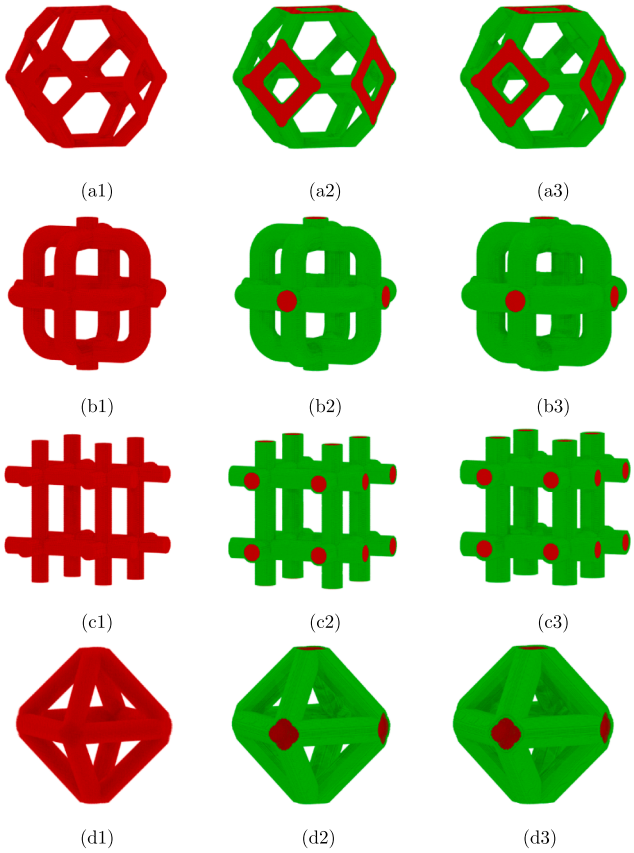

Fig. 2. Atomistic configurations of four different types of cell structures are shown from (a) to (d). The number 1 shows the pure copper structure, and the number 2 and 3 show the two composite core/shell structures with different thicknesses of 0.7 nm and 1.4 nm.

Table 1
Detailed information on different types of cell structures. Please note that the percentage of Cu and Ni atoms are both volume percentage.

Structure Name	Cu atoms (%)	Ni atoms (%)	Relative density (%)	Number of ligaments linked to joints
a1	100	0	6.97	4
a2	72.74	27.26	9.68	
a3	54.14	45.86	12.84	
b1	100	0	12.25	5
b2	78.17	21.83	15.68	
b3	61.23	38.77	20.01	
c1	100	0	10.06	6
c2	73.70	26.30	15.46	
c3	57.33	42.67	19.76	
d1	100	0	10.87	8
d2	74.16	25.84	14.66	
d3	58.32	41.68	18.65	

properties. A random nanofoam can then be modeled as a random distribution of geometric cells like the ones we consider in this paper. A specific mechanical property, such as the strength of the nanofoam, should fall within the range defined by the minimum – maximum strengths of the ordered nanofoams made with geometric representative cell structures.

First, a simulation box consisting of $150 \times 150 \times 150$ Cu lattice spacing with (0 0 1) direction was formed. For the pure copper nanofoams, the radius of the individual ligament was kept at 3 nm for all the cases. For the composite Cu/Ni nanofoams, two thin nickel layers of 0.7 nm and 1.4 nm were added to the previous pure copper ligaments to form the core/shell structure. These dimensions were chosen as a representative case to examine how the addition of the nickel layer can improve the mechanical behavior of the nanofoams. In this view, the effect of the ligament thickness, although important, has not been considered here. The cross-section views of the pure copper and the composite core/shell nanowires are shown in Fig. 1 using OVITO visualization software [34]. The atomistic configurations of the representative geometric cell structures are shown in Fig. 2. The detailed parameters of each cell structure are listed in Table 1. Overall, the total number of atoms in the simulations ranged from 0.8 million to 3.2 million with a relative density from around 0.07 to 0.20, depending on the structure.

2.2. Compression simulation using molecular dynamics

Molecular dynamics simulations were performed using LAMMPS [35] with the embedded atom method (EAM) [36,37]. The Voter and Chen [38] interatomic potential was used to describe the atomic interactions between Cu and Ni. Periodic boundary conditions were applied along all three directions to model infinitely large nanofoams. In all simulations, the temperature was kept constant to 300 K during both the relaxation and loading steps. The isothermal-isobaric (npt) ensemble was used to update the atomic velocities and positions at each step. The cell structures were subjected to three different types of compressive loading conditions, uniaxial, hydrostatic and mixed with a strain rate of 5×10^9 s^{-1}. For the mixed compression loading, the hydrostatic stress was first decreased to a fraction (3/4, 2/4 and 1/4) of the hydrostatic yield strengths, and a uniaxial compression was applied along z-direction until yield was achieved with the hydrostatic stress in the other two directions being kept constant. Using the yield points produced by the atomistic simulations yield surfaces were generated and curve fitted into the isotropic constitutive model suggested by Deshpande [27] to describe the multiaxial compressive behavior of the nanofoams. The yield function Φ is defined by:

$$\Phi \equiv \hat{\sigma} - Y \leq 0 \tag{1}$$

where the equivalent stress $\hat{\sigma}$ is:

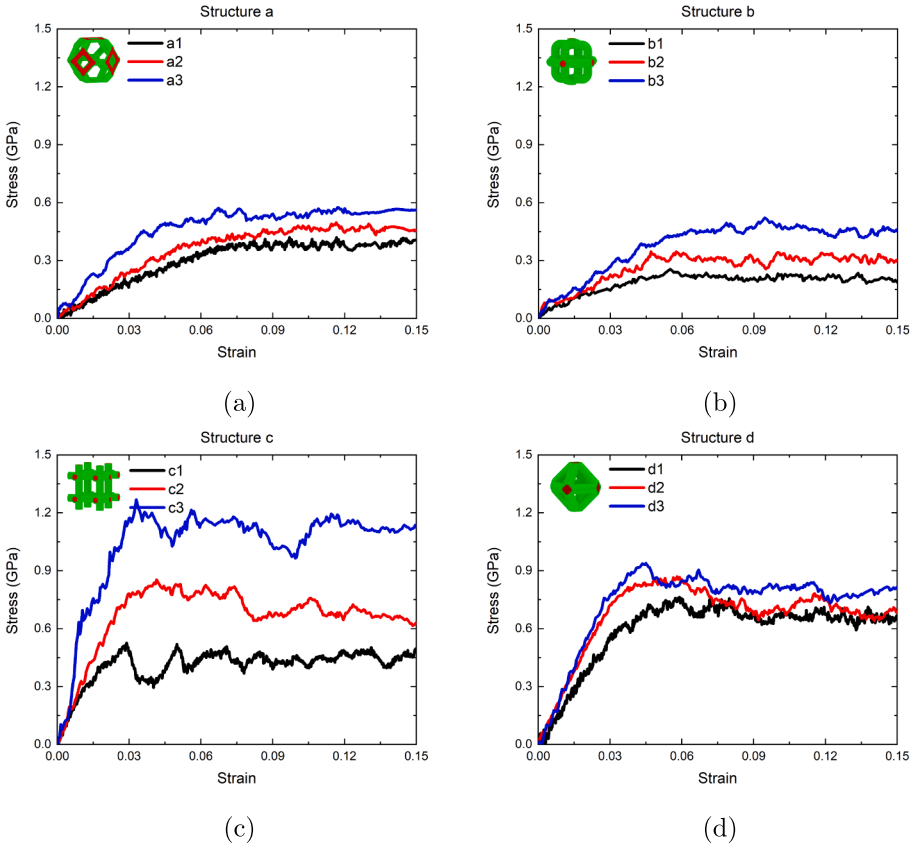

Fig. 3. The stress-strain curves of the four different types of cell structures during uniaxial compressive loading. The top left corner of each plot shows the shape of the cell structure. The black lines represent the pure copper behavior and the red and blue lines the core/shell composite behavior with nickel thicknesses of 0.7 nm and 1.4 nm, respectively.

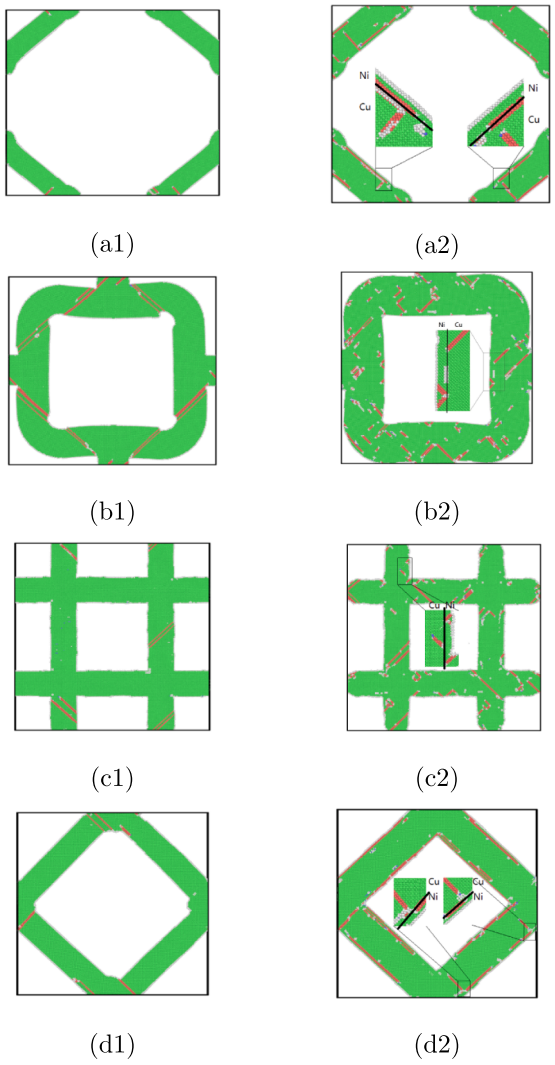

Fig. 4. Snapshots of the atomistic configuration of the pure copper (left column) and composite Cu/Ni ligament (right column) at the yield point during uniaxial compression. The nickel thicknesses are 1.4 nm for all four cell structures. The colors of the atoms represent their structure type calculated from the common neighbor analysis: green for FCC, red for HCP and grey for other structure types. (1) In the pure Cu case the dislocations propagate inside the whole ligament, (2) in the composite Cu/Ni case the dislocations stop at the interface as the magnification of the ligament in the inset at the center demonstrates.

$$\hat{\sigma}^2 \equiv \frac{1}{1+(\alpha/3)^2}[\sigma_e^2 + \alpha^2\sigma_m^2] \tag{2}$$

In Eq. (2), σ_m is the mean stress $\sigma_m \equiv \sigma_{kk}/3$ and σ_e is the von Mises effective stress $\sigma_e \equiv \sqrt{\frac{3}{2}\sigma_{ij}^2\sigma_{ij}^2}$. The mean stress and the von Mises effective stress were calculated at the yield point of all simulation tests. Then, both the mean stress and the effective stress are normalized with the uniaxial compressive yield strength to get the value of the parameter α, which defines the elliptical shape of the yield surface. The normalization of the yield stress used in this model makes it very suitable for its application with the molecular dynamics results that incorporate much higher strain rates than real experiments. The high strain rates result in higher yield stresses, but the normalization allows the implementation of this yield function even for this case.

2.3. Plasticity model

The hardening Y in Eq. (1) was suggested by Hanssen et al. [39]. This model has the advantage that it also includes the foam density, which is an important characteristic of the nanofoams.

$$Y = Y_o + \gamma\frac{\hat{\epsilon}}{\epsilon_D} + \alpha_2 \ln\left(\frac{1}{1-(\hat{\epsilon}/\epsilon_D)^\beta}\right) \tag{3}$$

In Eq. (3), Y_o is the yield strength, α_2, β and γ are material parameters, and ϵ_D is the compaction strain $\epsilon_D \equiv 1 - \frac{\rho_f}{\rho_o}$. Here, the first term Y_o represents the yield point, which is called plateau stress and is independent of the strain $\hat{\epsilon}$. The second term is the linear strain-hardening part. The strain hardening coefficient of γ defines the slope of the linear curve. The last term is the non-linear strain-hardening section where the stress-strain curve is determined by the scale factor α_2 and shape factor β. In this equation, the most important characteristic is that the strain hardening is a function of strain $\hat{\epsilon}$ relative to compaction strain ϵ_D, which indicates that the real-time nanofoam density plays a significant role in the strain hardening model.

3. Results

3.1. Molecular dynamics simulations

3.1.1. Stress-strain curves

Fig. 3 shows the stress-strain curves under uniaxial compression for the pure copper structures and composite Cu/Ni structures. In all cases, after the initial elastic deformation, the yield stress was reached. The yield stress depends on the geometry of the cell and, for the sample of pure copper, varies from about 0.25 to 0.5 GPa. The addition of the nickel layer increases the yield stress, which again depends on the geometry of the structure. More specifically, the yield strength of composite Cu/Ni cell has increased 36%, 107%, 198%, and 23% for types “a”, “b”, “c” and “d” respectively, compared to pure Cu cell structure. The increase is more evident in the case of the “c” arrangements with six ligaments per join and less apparent in the cases of “a” (four ligaments per join) and “d” (eight ligaments per join) structures. The “b” structures (five ligaments per join) stand in between the other two cases. This behavior can be attributed to the orientation of the ligaments to the loading direction. In the case of “c” (six ligaments per join), the straight perpendicular ligaments are parallel to the loading direction and can withstand more loading before deforming plastically without buckling. The “a” and “d” cells have ligaments angled to the loading direction, and they will exhibit some buckling before they deform plastically. Finally, structure “b” has ligaments parallel to the loading direction, that tend to resist the plastic deformation, and also exhibits some buckling due to its geometry that includes a join in the middle of the horizontal ligaments, thus combining the results of the other two cases.

All structures exhibit almost elastic-perfectly plastic behavior, which is consistent with the observed metallic foam performance at low strains [13]. The addition of the nickel shell layer, that coats the copper ligaments increases the overall strength of the structures since it acts as a barrier for the dislocation propagation. Fig. 4 shows the difference in dislocation behavior between a pure copper and a composite Cu/Ni ligament at the yield point. In the case of the pure copper ligaments, the dislocations are free to reach the free surface, while in the case of composite ligaments, the interface prevents the dislocations from moving (see the inset of Fig. 4).

In the case of composite ligaments, the dislocations first nucleate on the interface and move inside the copper layer. At low stresses, the interface acts as a barrier to dislocation transmission from the copper into the nickel layer, trapping them in the interface. As the stress increases, the dislocations begin to propagate also inside the nickel layer. This behavior has also been observed in the case of gold-nickel nanowires [18]. The interface barrier strength is determined by the stress field of the misfit dislocations at the interface and the Koehler image forces on the dislocations, as discussed in [40]. In our case, the

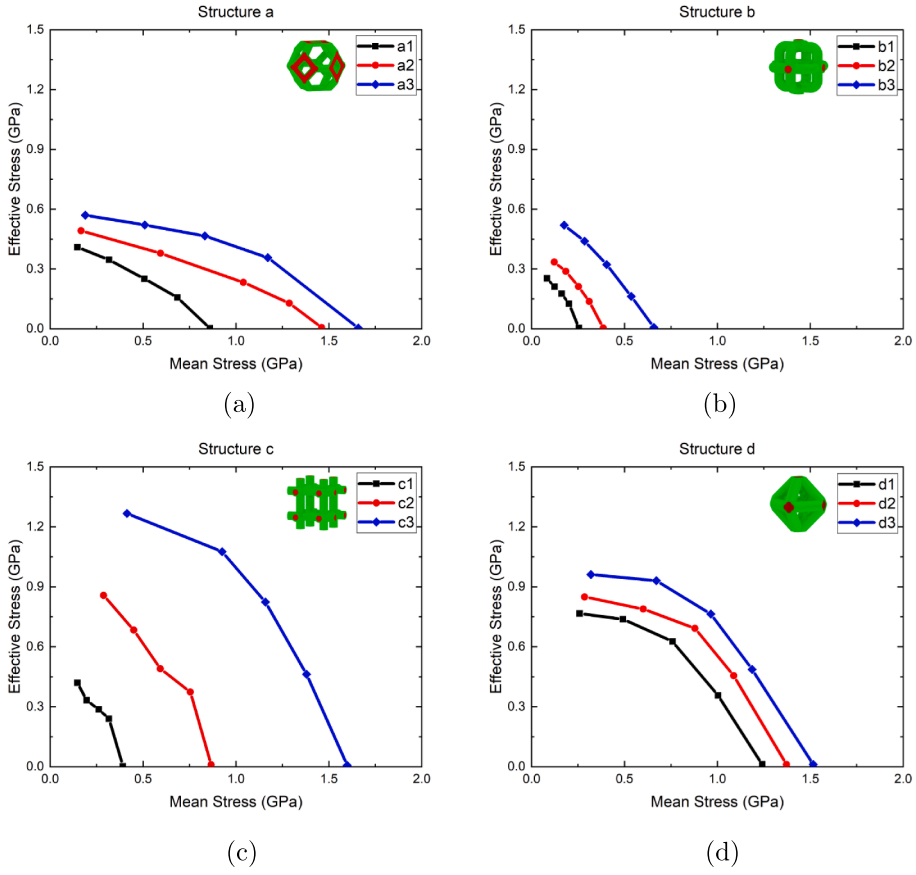

Fig. 5. Yield points of the four different types of cell structures. For all cases, the points with the highest effective stress represent the uniaxial compression test, and the points with no effective stress, the hydrostatic compression test. The other three points in-between represent the mixed compression tests.

Table 2
Uniaxial compressive yield strengths and the parameter α of different types of cell structures.

Structure type	Uniaxial yield strength (GPa)	α
a1	0.418	0.535
a2	0.489	0.363
a3	0.568	0.355
b1	0.251	1.104
b2	0.345	0.954
b3	0.521	0.893
c1	0.426	1.272
c2	0.852	1.176
c3	1.268	0.854
d1	0.763	0.645
d2	0.853	0.644
d3	0.938	0.641

dislocations in the Cu layer must overcome the repulsive image stresses from the Ni layer before slip can be transmitted across layers. This behavior results in stronger coated structures when compared to the single metal ones.

3.1.2. Yield surfaces

To obtain the yield surfaces for the four structures, the yield stress was calculated. We conducted five compression tests for each structure, including a pure uniaxial compression, a pure hydrostatic compression, and three combinations of hydrostatic and uniaxial compressions per the methodology discussed in the previous section. Fig. 5 shows the produced yield points for all the cell structures we considered in this work. The yield stresses in all cases increase with the addition of the nickel layers. The improvement depends on the thickness of the layer. For structures "a" and "d" is roughly doubled when the nickel layer thickness doubles. Again, structures "b" and "c" exhibit slightly larger increase in the yield strength with the increase of layer thickness, which is consistent to the previous discussion about the effect of their geometry to their strength. In all cases, the increase of yield stress results in a shift and expansion of the yield surfaces as Fig. 5 displays.

To curve fit the produced yield points to the theoretical model in Eq. (2), the mean and effective stresses must be normalized with the uniaxial compressive yield strength for each case as listed in Table 2. Fig. 6 shows the normalized yield points, and the resulted normalized yield surfaces. We must also note that for the uniaxial compression yield point in all structures, the normalized mean stresses are 1/3, and the normalized effective stresses are 1.0. Table 2 lists the values of obtained parameters α for each structure.

3.2. Continuum plasticity model

3.2.1. Validation of the constitutive model

The produced normalized yield surfaces from the previous section were then used to study the macroscopic behavior of pure copper and composite Cu/Ni nanofoams. Besides the yield function, a plasticity model also requires a hardening function to describe the plastic behavior of the materials after the first yield. In our case, Eq. (3) provided the required hardening behavior. This model has been already demonstrated its success in correctly predicting the macroscopic mechanical behavior of metallic nanofoams [39]. In Eq. (3) the phenomenological parameters α_2, γ, and $\frac{1}{\beta}$ must be found. These three material parameters depend on the relative density of the foam as defined by:

$$\left\{\alpha_2, \gamma, \frac{1}{\beta}\right\} = C_o + C_1\left(\frac{\rho_f}{\rho_o}\right)^n \tag{4}$$

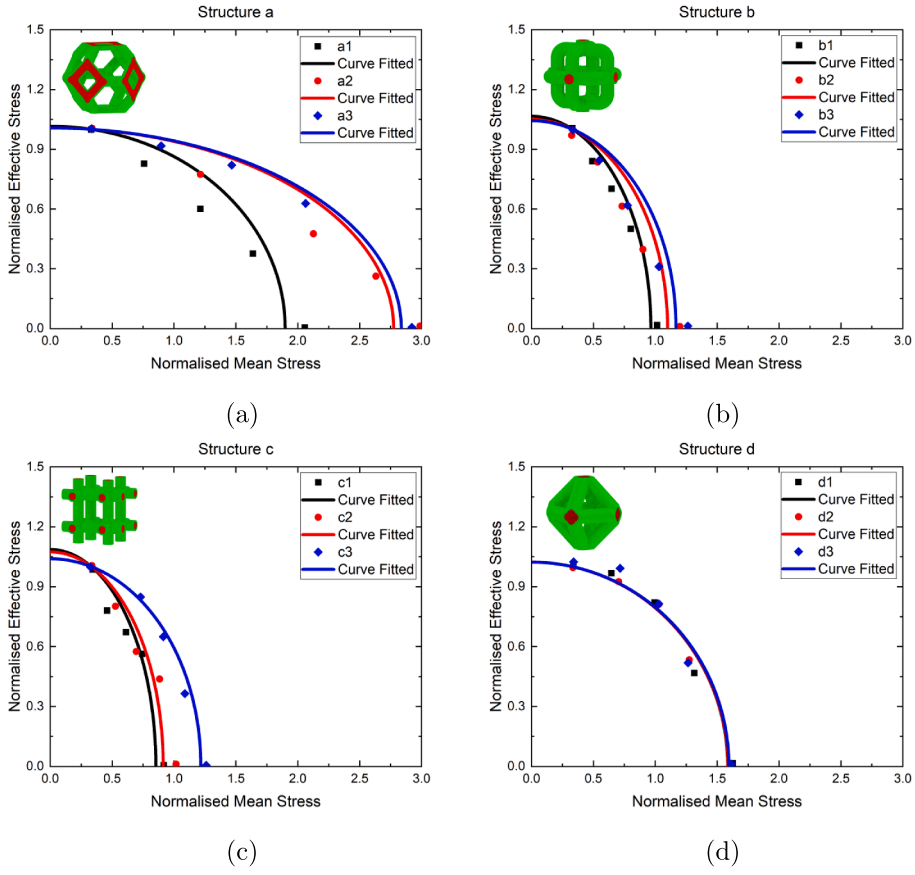

Fig. 6. Normalised yield surfaces of four different types of cell structures. Both the mean stresses and effective stresses are normalised by the uniaxial compressive yield strength.

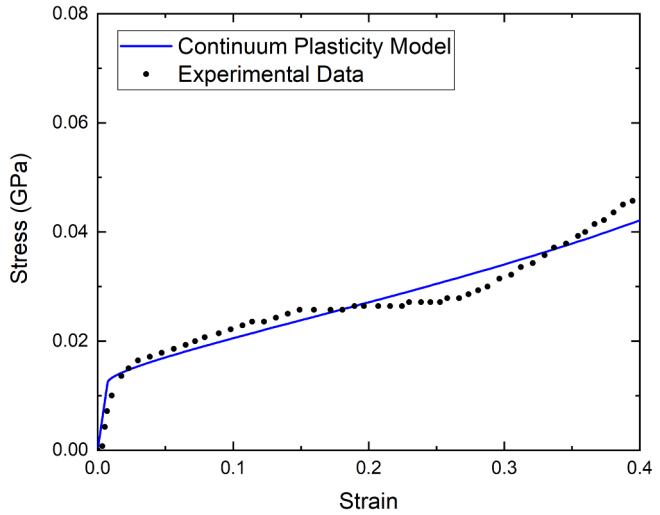

Fig. 7. Validation of the constitutive model. The experimental data are shown in black dots and the results from finite element method are shown in blue line.

where C_o, C_1, and n are constants. In this case, the three constants were determined by fitting experimental data on copper nanofoams during compression [41].

Finally, the complete plasticity model has been tested to find the stress-strain curve of a copper nanofoam of the same dimensions as the experimental samples and the corresponding density using the finite element method. The simulations were performed using MOOSE framework [42]. Fig. 7 shows the experimental data and numerical results. It is clear that the obtained finite element results match very well the experimental data; hence, this technique is able to get the macroscopic behavior of the metal nanofoam accurately.

Table 3
Parameters used for the different types of cell structures in the finite element analyses are listed to simulate the macroscopic compressive behavior of Cu nanofoams.

Structure Name	α_2 (MPa)	β	γ (MPa)	E (MPa)	Y_o (MPa)	ϵ_D
a1	12.70	3.07	12.69	602	10.0	0.9303
a2	12.74	2.54	12.73	1374	11.7	0.9032
a3	12.78	2.04	12.77	2672	13.6	0.8716
b1	12.78	2.12	12.76	1861	23.0	0.8775
b2	12.81	1.70	12.80	3494	31.6	0.8432
b3	12.85	1.31	12.83	6253	47.7	0.7999
c1	12.75	2.47	12.74	1255	17.5	0.8994
c2	12.81	1.72	12.79	3485	35.0	0.8454
c3	12.85	1.33	12.83	6225	52.1	0.802
d1	12.76	2.33	12.75	1465	19.6	0.8913
d2	12.80	1.81	12.79	3126	21.9	0.8534
d3	12.84	1.41	12.82	5516	23.3	0.8135

3.2.2. *Plateau stress and elastic modulus*

To fully apply the above plasticity model, the plateau stress and the elastic modulus must be known, since they determine the overall mechanical behavior of the foam. The plateau stress corresponds to the initial yield stress Y_o. For the nanofoams a scaling equation has been proposed [14]:

$$\sigma_p = C_2\sigma_s\left(\frac{\rho_f}{\rho_o}\right)^{\frac{3}{2}} \tag{5}$$

where σ_s is the yield strength for the bulk material, C_2 is a material

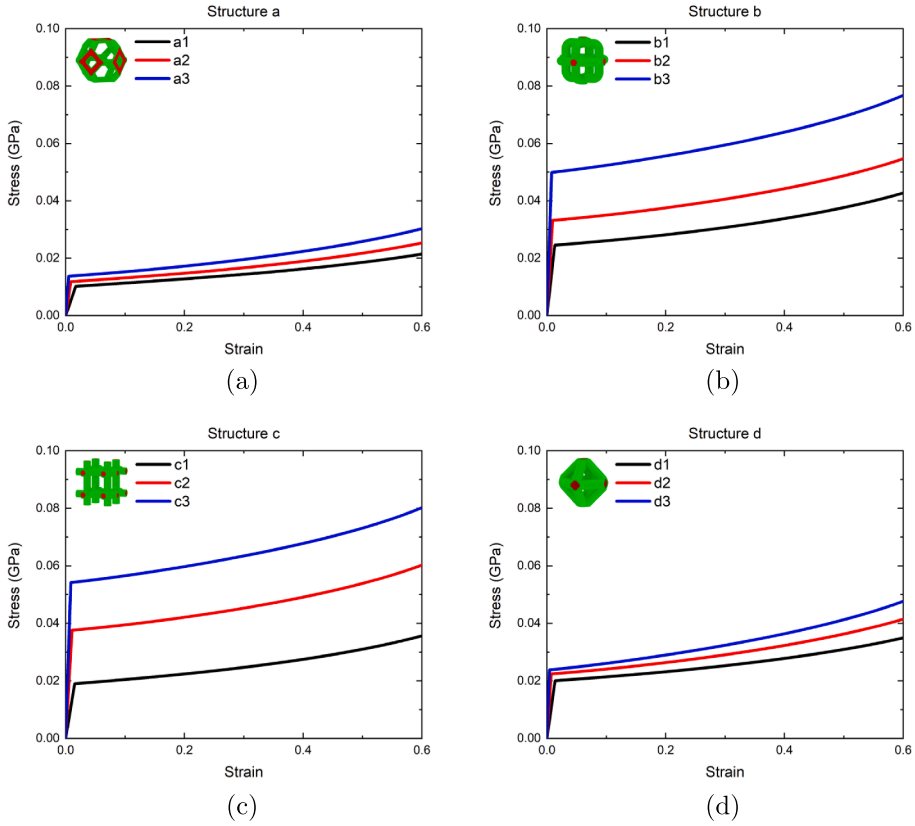

Fig. 8. Macroscopic stress/strain curve of four different types of Cu nanofoams.

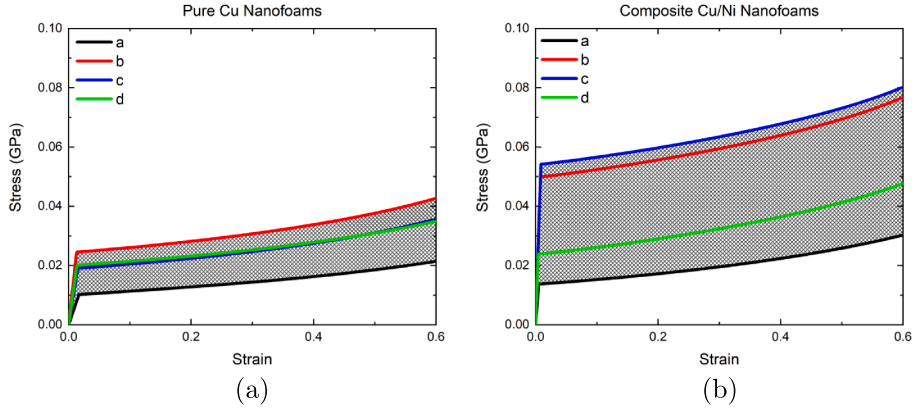

Fig. 9. Ranges of stress/strain curves of specific pure Cu nanofoams and composite Cu/Ni nanofoams are shown in (a) and (b), respectively. The relative density for the pure Cu nanfoams is from 6.97% to 12.25%, and the relative density for the composite Cu/Ni nanofoams is from 12.84% to 20.01%.

constant and (ρ_f/ρ_o) is the relative density of the nanofoam. Also, the yield strength depends on the grain size [39], which in our case corresponds to the ligament size:

$$\sigma_s = \sigma_o + k_1 D^{-1/2} \tag{6}$$

where σ_o and k_1 are Hall-Petch parameters taken from literature.

Using Eqs. (5) and (6) above, we can calculate the plateau strength of pure copper nanofoams for different relative densities. Due to lack of both experimental results and theoretical findings on composite Cu/Ni nanofoams, the necessary plateau stresses were calculated using the ratio of the copper yield stress over the Cu/Ni yield stress taken from the atomistic simulations for the uniaxial compression and each case, see Fig. 5.

The elastic modulus of the pure copper nanofoam was determined using the scaling equation [13]:

$$E = E_o \left(\frac{\rho_f}{\rho_o}\right)^2 \tag{7}$$

where E_o is the elastic modulus of bulk Cu. For the elastic modulus of the composite Cu/Ni nanofoams, we are using the general rule of mixtures like in [10] for the relative densities listed in Table 1.

3.2.3. Macroscopic stress-strain curves for Cu nanofoams

Table 3 lists the parameters required for the finite element analyses of each structure as obtained by the methodology described in the previous paragraphs for all cell arrangements. The produced stress-strain curves of the single copper and composite Cu/Ni nanofoams, with the representative volume element being the structures “a”–“d”, are shown in Fig. 8. The results suggest that the addition of the nickel coating improves the mechanical behavior of the metallic nanofoam.

The improvement depends on the geometry of the unit cell structure we consider. The results represent the mechanical behavior of ordered metal nanofoams since the same unit structure is repeatedly used in every integration point. In the case of random nanofoams, this will not occur, as the geometry and the relative density could vary at every integration point. Therefore, the results in Fig. 8 will provide ranges of stress-strain curves since a random metal nanofoam can be approximated as a collection of all the unit cell geometries randomly distributed inside the macroscopic structure. By changing the percentage amount of each unit cell, we can get the potential ranges of the stress-strain curve of a specific nanofoam as demonstrated in Fig. 9.

4. Conclusion

In this work, we presented a multiscale approach to predict the mechanical properties of Cu nanofoams. Four specific types of nanofoam cell structures have been constructed and distinguished by the number of ligaments connected to one joint. Then, the yield surface of these structures was generated using molecular dynamics, and the results were curve fitted into a yield equation that incorporated both the mean and effective stresses. Finally, the finite element method has been implemented to simulate the macroscopic mechanical behavior of Cu nanofoams under uniaxial compression test. Overall, the nickel-coated copper nanofoams are much stronger than their pure copper counterparts under compression. The architecture of the morphology could have significant impacts on the mechanical properties of the Cu nanofoams. The application of this method can be used to provide further insights in predicting and optimizing the mechanical behavior of macroscopic nanofoam specimens under complex loading conditions.

CRediT authorship contribution statement

H. Ke: Conceptualization, Methodology, Software, Validation, Formal analysis, Resources, Data curation, Writing - original draft, Visualization. **A. Garcia Jimenez:** Methodology, Software, Software, Formal analysis, Data curation, Writing - original draft. **D.A. Rodrigues Da Silva:** Software, Visualization. **I. Mastorakos:** Conceptualization, Methodology, Investigation, Writing - review & editing, Supervision, Project administration, Funding acquisition.

Declaration of Competing Interest

None.

Acknowledgment

This work was supported by the National Science Foundation under Grant No. CMMI-MEP-1634640.

References

[1] S. Bhaviripudi, E. Mile, S.A. Steiner, A.T. Zare, M.S. Dresselhaus, A.M. Belcher, J. Kong, Cvd synthesis of single-walled carbon nanotubes from gold nanoparticle catalysts, J. Am. Chem. Soc. 129 (2007) 1516–1517 PMID:17283991.
[2] S. Sen, D. Liu, G.T.R. Palmore, Electrochemical reduction of co2 at copper nanofoams, ACS Catal. 4 (2014) 3091–3095.
[3] B. Soni, S. Biswas, Processing of open-cell metallic foams for high pressure hydrogen storage, Trans. Indian Inst. Met. 70 (2017) 1921–1931.
[4] S. Mellouli, H. Dhaou, F. Askri, A. Jemni, S.B. Nasrallah, Hydrogen storage in metal hydride tanks equipped with metal foam heat exchanger, Int. J. Hydrogen Energy 34 (2009) 9393–9401.
[5] C.-J. Tseng, B.T. Tsai, Z.-S. Liu, T.-C. Cheng, W.-C. Chang, S.-K. Lo, A pem fuel cell with metal foam as flow distributor, Energy Convers. Manage. 62 (2012) 14–21.
[6] M. Kim, C. Kim, Y. Sohn, Application of metal foam as a flow field for pem fuel cell stack, Fuel Cells 18 (2018) 123–128.
[7] J. Biener, G.W. Nyce, A.M. Hodge, M.M. Biener, A.V. Hamza, S.A. Maier, Nanoporous plasmonic metamaterials, Adv. Mater. 20 (2008) 1211–1217.
[8] S. Yun, Y. Qin, A.R. Uhl, N. Vlachopoulos, M. Yin, D. Li, X. Han, A. Hagfeldt, New-generation integrated devices based on dye-sensitized and perovskite solar cells, Energy Environ. Sci. 11 (2018) 476–526.
[9] J. Biener, A.M. Hodge, A.V. Hamza, Microscopic failure behavior of nanoporous gold, Appl. Phys. Lett. 87 (2005) 121908.
[10] C.-E. Kim, R.M. Rahimi, N. Hightower, I. Mastorakos, D.F. Bahr, Synthesis, microstructure, and mechanical properties of polycrystalline Cu nano-foam, MRS Adv. (2018) 1–7.
[11] L. He, N. Abdolrahim, Deformation mechanisms and ductility enhancement in core-shell cu-ni nanoporous metals, Comput. Mater. Sci. 150 (2018) 397–404.
[12] N. Abdolrahim, D.F. Bahr, B. Revard, C. Reilly, J. Ye, T.J. Balk, H.M. Zbib, The mechanical response of core-shell structures for nanoporous metallic materials, Philos. Mag. 93 (2013) 736–748.
[13] L.J. Gibson, M.F. Ashby, Cellular Solids: Structure and Properties, second ed., Cambridge Solid State Science Series, Cambridge University Press, 1997.
[14] A. Hodge, J. Biener, J. Hayes, P. Bythrow, C. Volkert, A. Hamza, Scaling equation for yield strength of nanoporous open-cell foams, Acta Mater. 55 (2007) 1343–1349.
[15] H. Fan, D. Fang, Modeling and limits of strength of nanoporous foams, Mater. Des. 30 (2009) 1441–1444.
[16] R. Xia, X. Li, Q. Qin, J. Liu, X.-Q. Feng, Surface effects on the mechanical properties of nanoporous materials, Nanotechnology 22 (2011) 265714.
[17] X.-Q. Feng, R. Xia, X. Li, B. Li, Surface effects on the elastic modulus of nanoporous materials, Appl. Phys. Lett. 94 (2009) 011916.
[18] H. Ke, I. Mastorakos, Deformation behavior of core-shell nanowire structures with coherent and semi-coherent interfaces, J. Mater. Res. 34 (2019) 1093–1102.
[19] A. Misra, J.P. Hirth, H. Kung, Single-dislocation-based strengthening mechanisms in nanoscale metallic multilayers, Philos. Mag. A 82 (2002) 2935–2951.
[20] C. Henager, R. Hoagland, A rebound mechanism for misfit dislocation creation in metallic nanolayers, Scr. Mater. 50 (2004) 701–705.
[21] F. Akasheh, H.M. Zbib, J.P. Hirth, R.G. Hoagland, A. Misra, Dislocation dynamics analysis of dislocation intersections in nanoscale metallic multilayered composites, J. Appl. Phys. 101 (2007) 084314.
[22] F. Akasheh, H.M. Zbib, S. Akarapu, C. Overman, D. Bahr, Multiscale modeling of dislocation mechanisms in nanoscale multilayered composites, MRS Proc. 1130 (2008) 1130-W13-01.
[23] I.N. Mastorakos, H.M. Zbib, D.F. Bahr, Deformation mechanisms and strength in nanoscale multilayer metallic composites with coherent and incoherent interfaces, Appl. Phys. Lett. 94 (2009) 173114.
[24] N. Abdolrahim, I. Mastorakos, H. Zbib, Precipitate strengthening in nanostructured metallic material composites, Philos. Mag. Lett. 92 (2012) 597–607.
[25] N. Abdolrahim, H.M. Zbib, D.F. Bahr, Multiscale modeling and simulation of deformation in nanoscale metallic multilayer systems, Int. J. Plasticity 52 (2014) 33–50 In Honor of Hussein Zbib.
[26] I. Mastorakos, N. Abdolrahim, H. Zbib, Deformation mechanisms in composite nano-layered metallic and nanowire structures, Int. J. Mech. Sci. 52 (2010) 295–302 SPECIAL ISSUE: Advances in Modeling and Evaluation of Materials in Honor of Professor Tomita.
[27] V. Deshpande, N. Fleck, Isotropic constitutive models for metallic foams, J. Mech. Phys. Solids 48 (2000) 1253–1283.
[28] N. Gunkelmann, Y. Rosandi, C.J. Ruestes, E.M. Bringa, H.M. Urbassek, Compaction and plasticity in nanofoams induced by shock waves: a molecular dynamics study, Comput. Mater. Sci. 119 (2016) 27–32.
[29] N. Gunkelmann, E.M. Bringa, Y. Rosandi, Molecular dynamics simulations of aluminum foams under tension: influence of oxidation, J. Phys. Chem. C 122 (2018) 26243–26250.
[30] H. Ke, A.G. Jimenez, I. Mastorakos, A multiscale approach to predict the mechanical properties of copper nanofoams 4 (2019) 293–298.
[31] D.A. Crowson, D. Farkas, S.G. Corcoran, Geometric relaxation of nanoporous metals: the role of surface relaxation, Scr. Mater. 56 (2007) 919–922.
[32] D.A. Crowson, D. Farkas, S.G. Corcoran, Mechanical stability of nanoporous metals with small ligament sizes, Scr. Mater. 61 (2009) 497–499.
[33] B.-N.D. Ngô, A. Stukowski, N. Mameka, J. Markmann, K. Albe, J. Weissmüller, Anomalous compliance and early yielding of nanoporous gold, Acta Mater. 93 (2015) 144–155.
[34] A. Stukowski, Visualization and analysis of atomistic simulation data with OVITO–the open visualization tool, Modell. Simul. Mater. Sci. Eng. 18 (2009) 015012.
[35] S. Plimpton, Fast parallel algorithms for short-range molecular dynamics, J. Comput. Phys. 117 (1995) 1–19.
[36] M.S. Daw, M.I. Baskes, Embedded-atom method: derivation and application to impurities, surfaces, and other defects in metals, Phys. Rev. B 29 (1984) 6443–6453.
[37] M.S. Daw, S.M. Foiles, M.I. Baskes, The embedded-atom method: a review of theory and applications, Mater. Sci. Rep. 9 (1993) 251–310.
[38] A.F. Voter, S.P. Chen, Accurate interatomic potentials for ni, al and ni3al, MRS Proc. 82 (1986) 175.
[39] A. Hanssen, O. Hopperstad, M. Langseth, H. Ilstad, Validation of constitutive models applicable to aluminium foams 44 (2002) 359–406.
[40] A. Misra, H. Krug, Deformation behavior of nanostructured metallic multilayers, Adv. Eng. Mater. 3 (2001) 217–222.
[41] J. Gubicza, P. Jenei, K. Nam, C. Kádár, H. Jo, H. Choe, Compressive behavior of cu-ni alloy foams: effects of grain size, porosity, pore directionality, and chemical composition, Mater. Sci. Eng.: A 725 (2018) 160–170.
[42] D.R. Gaston, C.J. Permann, J.W. Peterson, A.E. Slaughter, D. Andrš, Y. Wang, M.P. Short, D.M. Perez, M.R. Tonks, J. Ortensi, L. Zou, R.C. Martineau, Physics-based multiscale coupling for full core nuclear reactor simulation, Ann. Nucl. Energy 84 (2015) 45–54 Multi-Physics Modelling of LWR Static and Transient Behaviour.